

Mn, Cu, and Zn abundances in barium stars and their correlations with neutron capture elements^{★,★★,★★★}

D. M. Allen¹ and G. F. Porto de Mello²

¹ Instituto de Astronomia, Geofísica e Ciências Atmosféricas, Universidade de São Paulo, Rua do Matão 1226, CEP: 05508-900, São Paulo, Brazil

e-mail: dimallen@astro.iag.usp.br

² Universidade Federal do Rio de Janeiro, Observatório do Valongo, Ladeira do Pedro Antonio 43, CEP: 20080-090, Rio de Janeiro, RJ, Brazil

e-mail: gustavo@astro.ufrj.br

Received; accepted

ABSTRACT

Barium stars are optimal sites for studying the correlations between the neutron-capture elements and other species that may be depleted or enhanced, because they act as neutron seeds or poisons during the operation of the *s*-process. These data are necessary to help constrain the modeling of the neutron-capture paths and explain the *s*-process abundance curve of the solar system. Chemical abundances for a large number of barium stars with different degrees of *s*-process excesses, masses, metallicities, and evolutionary states are a crucial step towards this goal. We present abundances of Mn, Cu, Zn, and various light and heavy elements for a sample of barium and normal giant stars, and present correlations between abundances contributed to different degrees by the weak-*s*, main-*s*, and *r*-processes of neutron capture, between Fe-peak elements and heavy elements. Data from the literature are also considered in order to better study the abundance pattern of peculiar stars. The stellar spectra were observed with FEROS/ESO. The stellar atmospheric parameters of the eight barium giant stars and six normal giants that we analyzed lie in the range $4300 < T_{\text{eff}}/\text{K} < 5300$, $-0.7 < [\text{Fe}/\text{H}] \leq 0.12$ and $1.5 \leq \log g < 2.9$. Carbon and nitrogen abundances were derived by spectral synthesis of the molecular bands of C₂, CH, and CN. For all other elements we used the atomic lines to perform the spectral synthesis. A very large scatter was found mainly for the Mn abundances when data from the literature were considered. We found that [Zn/Fe] correlates well with the heavy element excesses, its abundance clearly increasing as the heavy element excesses increase, a trend not shown by the [Cu/Fe] and [Mn/Fe] ratios. Also, the ratios involving Mn, Cu, and Zn and heavy elements usually show an increasing trend toward higher metallicities. Our results suggest that a larger fraction of the Zn synthesis than of Cu is owed to massive stars, and that the contribution of the main-*s* process to the synthesis of both elements is small. We also conclude that Mn is mostly synthesized by SN Ia, and that a non-negligible fraction of the synthesis of Mn, Cu, and Zn is owed to the weak *s*-process.

Key words. stars: chemically peculiar – stars: abundances – stars: late-type – techniques: spectroscopic

1. Introduction

It is becoming increasingly clear in the present age of high-resolution spectroscopy of large databases and precise abundances for numerous chemical elements that the galactic chemical evolution (GCE) models are lacking with regard to the available observational data. A successful GCE model must incorporate stellar evolution inputs such as an initial mass function, star-formation rate, mass loss through winds and eruptive processes, and also differing timescales for stellar nucleosynthetic yields and their sensitivities to differing metallicities. It must also link these to the complexities of dynamical galactic components and the great diversity of observed structures, in which formation, dissolution, and merging processes labor many hi-

erarchical levels. Such a model is largely lacking, and it must involve a sufficiently large number of still essentially constraint-free parameters that the most stringent challenges presently rest on the theoretical side, instead of the observational one.

A good example of this state of affairs is the nucleosynthesis of Mn, Cu, and Zn. The astrophysical sites of, timescales of, and dominant contributing processes to the synthesis of the Fe-peak element Mn, a classical Fe-peak element, and Cu and Zn, considered to be the lightest *s*-process main component nuclei and the heaviest Fe-peak element respectively, still have not been reliably established. A theoretical and observational debate is still on-going to determine the expected main contributors to the observed Mn abundances, whether type II or type Ia supernovae (SNe), and to establish if the Mn yields depend on the metallicity of the SN progenitors (Feltzing et al. 2007; Nissen et al. 2000).

Cu and Zn are part of an even more complex scenario. They have traditionally been considered as transition elements between the Fe-peak and the light *s*-process species (Snedden et al. 1991). They are thought to be produced through a variety of nucleosynthetic processes, including explosive nucleosynthesis in SN II and SN Ia, the main component of the *s*-process, thought to occur in the He-burning shells of low to intermediate mass AGB stars, and the weak component of the *s*-process, thought to be

* Based on spectroscopic observations collected at the European Southern Observatory (ESO), within the Observatório Nacional ON/ESO and ON/IAG agreements, under FAPESP project n° 1998/10138-8.

** Tables 2 and 3, are only available in electronic form at the CDS via anonymous ftp to cdsarc.u-strasbg.fr (130.79.128.5) or via <http://cdsweb.u-strasbg.fr/cgi-bin/qcat?J/A+A/>

*** Figures 1, 2, 3, 4, 5, 7, and 8 and Tables 1, 6, and 7 are only available in electronic form at <http://www.edpsciences.org>

sited at He-burning cores of $M \geq 10 M_{\odot}$ stars (see Raiteri et al. 1993; Matteucci et al. 1993; Mishenina et al. 2002, and references therein). Even though their positions in the periodic table are contiguous, their behavior in the GCE scenario is in sharp contrast.

The solar curves for the abundance of s -only nuclei vs. mass number of Käppeler et al. (1989) show that the observational data very well fit the theoretical curve for nuclei from $A > 90$, whereas for lighter nuclei another process is necessary to explain the solar abundances. This process was called the weak component of the s -process, whose reproduction by successive stellar generations was investigated taking into account the interference of the main component in the atomic mass range from Fe to Sr, and a satisfactory match to the solar s -abundance was reached. Lamb et al. (1977) studied the contribution of the weak component for nuclei lighter than Fe and found that significant amounts of some elements with $A < 60$ are produced in stars with $M < 15 M_{\odot}$ and that nuclei in the atomic range $60 \leq A \leq 70$ are made in stars more massive than about $15 M_{\odot}$.

Given the very intricate scenario for the nucleosynthesis of Mn, Cu, and Zn, additional abundance data from as many nucleosynthetic sources as possible are expected to contribute to the quantification of the various processes at play. Our aim in this paper is to help clarify the nucleosynthetic processes that contribute to the production of Mn, Cu, and Zn by comparing their abundances in a sample of barium dwarf and giant stars to the abundances of heavy elements. Barium stars show high excesses of the elements produced by the main s -process. Because they are not evolved enough to have self-enriched in these elements, a binary nature is invoked to explain their existence (McClure et al. 1980). Thus, chemical peculiarities of the barium stars come from a more massive companion, presently observed (if at all) as a white dwarf. It evolved faster and, as a thermally pulsating AGB, became self-enriched with products of the main s -process, thereby transferring this enriched material onto the current barium star after dredge-up episodes through a stellar wind. These overabundances, then, are not intrinsic to the barium star, can be directly linked to the AGB nucleosynthesis, and therefore are important tests of the theories of nucleosynthesis and the chemical evolution of the Galaxy. The main goal of our effort is to provide new observational constraints to the chemical evolution of Mn, Cu, and Zn by gauging the effects on these elements of s -process nucleosynthesis in heavy-element enhanced stars.

The paper is organized as follows: Section 2 briefly presents the data and the determination of the stellar atmospheric parameters; Sect. 3 briefly describes the abundance and uncertainty determinations; in Sect. 4 the correlations between the Mn, Cu, and Zn abundances and those of the neutron capture elements are discussed, and in Sect. 5 we draw our conclusions.

2. Observations and atmospheric parameters

All spectra for the sample stars were obtained with the 1.52m telescope at ESO, La Silla, using the Fiber Fed Extended Range Optical Spectrograph (FEROS, Kaufer et al. 2000). FEROS spectra have a constant resolving power of $R = 48000$ from 3600 Å to 9200 Å. The stellar sample targeted in our study includes eight mild and classical barium stars and six normal giants of Smiljanic et al. (2007), with a spectral S/N ratio ranging from 200 to 450 in the visible range.

Smiljanic et al. (2007) determined T_{eff} , $\log g$, and the metallicities from the simultaneous excitation and ionization equilibria of the equivalent widths of an average number of 120 Fe I

Table 2. Lines, equivalent widths, and abundances. Abundances of Mn for barium stars from Allen & Barbuy (2006a) are shown starting on line 1541. Note that HD 2454 is HR 107 in Allen & Barbuy (2006a). The full table is only available in CDS.

Star	El	λ (Å)	χ_{ex} (eV)	$\log gf$	Ref	EW (mÅ)	$\log \epsilon$	[X/Fe]
HD 9362*	Li I**	6707.760	0.000	0.171	1	...	-0.34	...
HD 9362*	Li I**	6707.910	0.000	-0.299	2	...	-0.34	...
HD 9362*	Li I**	6708.087	0.000	0.000	3	...	-0.34	...
HD 9362*	C	4295.000a	8.16	-0.02
HD 9362*	C	5135.600b	8.19	0.01

Notes. “*” indicates stars that were considered to be normal instead of barium stars by Smiljanic et al. (2007), and the well-known giant ϵ Vir (HD 113226), used by them as reference star; “**” indicates multiple line; “a”: representative line for CH (G band); “b”: representative line for C₂; “c”: representative line for CN. < indicates an upper limit. The gf -values sources are given below.

References. (1) McWilliam & Rich (1994); (2) NIST; (3) Barbuy et al. (1999); (4) Allende Prieto et al. (2001); (5) Lambert (1978); (6) Bielski (1975); (7) Biémont & Godefroid (1980); (8) Gratton & Sneden (1994); (9) Hannaford et al. (1982); (10) Hannaford & Lowe (1983); (11) Biémont et al. (1981); (12) Thévenin (1990); (13) Thévenin (1989); (14) Smith et al. (2000); (15) VALD; (16) McWilliam (1998); (17) Rutten (1978); (18) Lawler et al. (2001a); (19) Palmeri et al. (2000); (20) Goly et al. (1991); (21) Lage & Whaling (1976); (22) Hartog et al. (2003); (23) Maier & Whaling (1977); (24) Sneden et al. (1996); (25) Biémont et al. (1989); (26) Lawler et al. (2001b); (27) Bergstrom et al. (1988); (28) Corliss & Bozman (1962); (29) average between Kusz (1992) and Biémont & Lowe (1993); (30) Biémont et al. (2000); “SUN” indicates $\log gf$ obtained through fits on the solar spectrum.

Table 3. Average for $\log \epsilon(X)$ and [X/Fe]. Uncertainties on $\log \epsilon(X)$ and [X/Fe] are represented by σ_l and σ_f , respectively. Given that Smiljanic et al. (2007) used HD 113226 as a reference star, there is no uncertainty designed to it. The full table is only available in CDS.

Star	El	$\log \epsilon(X)$	[X/Fe]	σ_l	σ_f
HD 9362*	Li	-0.34	...	0.14	0.16
HD 9362*	C	8.19	0.01	0.10	0.10
HD 9362*	N	7.73	0.15	0.09	0.08
HD 9362*	O	8.54	0.14	0.17	0.17
HD 9362*	Mn	4.80	-0.25	0.11	0.10
HD 9362*	Cu	3.66	-0.21	0.12	0.11
HD 9362*	Zn	4.01	-0.25	0.13	0.13

Notes. The symbol “*” indicates those stars that were considered to be normal instead of barium stars by Smiljanic et al. (2007). From the line 351, the data of Allen & Barbuy (2006a) with corrected uncertainties are shown. From the line 1001, the solar abundances and their references are shown.

and 12 Fe II lines. Surface gravities were also computed from the stellar luminosities and theoretical HR diagrams, and a very good agreement was found for the two sets of gravities. A summary of the stellar parameters is given in Table 1. The reader is referred to Smiljanic et al. (2007) for a journal of the observations, details of derivation of atmospheric parameters, and the respective uncertainties.

Additionally, we determined the Mn abundances for the 26 Ba stars analyzed by Allen & Barbuy (2006a), to whom we refer the reader for details on observations and the derivation of atmospheric parameters.

Table 4. Hyperfine structure for Mn I and Cu I lines.

ID	λ (Å)	log gf	ID	λ (Å)	log gf
4754.042 Å; $\chi_{ex}=2.282$ eV log gf (total) = -0.086 ^a			6021.792 Å; $\chi_{ex}=3.075$ eV log gf (total) = -0.216 ^a		
Mn I	4754.0210	-0.6523	Mn I	6021.7190	-2.6674
Mn I	4754.0320	-0.7918	Mn I	6021.7450	-1.4499
Mn I	4754.0420	-0.9502	Mn I	6021.7480	-2.3152
Mn I	4754.0520	-1.1342	Mn I	6021.7680	-1.2739
Mn I	4754.0540	-1.5699	Mn I	6021.7710	-2.1903
Mn I	4754.0600	-1.3561	Mn I	6021.7760	-0.5323
Mn I	4754.0600	-1.3939	Mn I	6021.7870	-1.2483
Mn I	4754.0640	-1.3683	Mn I	6021.7910	-2.2695
Mn I	4754.0660	-1.6413	Mn I	6021.7940	-0.6718
Mn I	4754.0680	-1.4352	Mn I	6021.8000	-1.3152
Mn I	4754.0710	-1.6113	Mn I	6021.8070	-0.8302
Mn I	4754.0800	-2.3895	Mn I	6021.8100	-1.4913
Mn I	4754.0820	-2.3103	Mn I	6021.8160	-1.0142
Mn I	4754.0820	-2.4352	Mn I	6021.8200	-1.2361
Mn I	4754.0820	-2.7874	Mn I	6021.8200	-1.5213
5420.350 Å; $\chi_{ex}=2.143$ eV log gf (total) = -1.460 ^a			5105.50 Å; $\chi_{ex}=1.39$ eV log gf (total) = -1.520 ^b		
Mn I	5420.2600	-3.0163	Cu I	5105.497	-4.2291
Mn I	5420.2650	-2.9863	Cu I	5105.501	-3.2774
Mn I	5420.2730	-2.7311	Cu I	5105.503	-3.2314
Mn I	5420.2730	-3.7645	Cu I	5105.504	-4.4202
Mn I	5420.2820	-2.8102	Cu I	5105.510	-3.1656
Mn I	5420.2960	-2.5092	Cu I	5105.514	-2.9097
Mn I	5420.2960	-3.6853	Cu I	5105.519	-3.8761
Mn I	5420.3090	-2.7433	Cu I	5105.523	-2.9318
Mn I	5420.3270	-2.3252	Cu I	5105.525	-2.7319
Mn I	5420.3280	-3.8102	Cu I	5105.526	-4.0655
Mn I	5420.3450	-2.7689	Cu I	5105.530	-2.6600
Mn I	5420.3680	-2.1668	Cu I	5105.531	-2.8199
Mn I	5420.3690	-4.1624	Cu I	5105.534	-2.5629
Mn I	5420.3910	-2.9449	Cu I	5105.545	-2.9140
Mn I	5420.4180	-2.0273	Cu I	5105.550	-2.3138
			Cu I	5105.554	-2.4538
			Cu I	5105.572	-2.1079
5432.548 Å; $\chi_{ex}=0.000$ eV log gf (total) = -3.795 ^a			5218.21 Å; $\chi_{ex}=3.82$ eV log gf (total) = +0.264 ^a		
Mn I	5432.5080	-4.3769	Cu I	5218.201	-1.4123
Mn I	5432.5120	-5.1550	Cu I	5218.203	-0.9367
Mn I	5432.5370	-5.1550	Cu I	5218.205	-1.0665
Mn I	5432.5400	-4.6401	Cu I	5218.207	-0.3466
Mn I	5432.5430	-4.9923	Cu I	5218.211	-0.5575
Mn I	5432.5620	-4.9923	Cu I	5218.213	-0.5685
Mn I	5432.5650	-4.9711	Cu I	5218.216	-0.2226
Mn I	5432.5670	-4.9869			
Mn I	5432.5820	-4.9869			
Mn I	5432.5840	-5.4182			
Mn I	5432.5860	-5.0892			
Mn I	5432.5950	-5.0892			
Mn I	5432.5970	-6.1172			
Mn I	5432.5980	-5.3513			
Mn I	5432.6030	-5.3513			
6013.488 Å; $\chi_{ex}=3.072$ eV log gf (total) = -0.252 ^a			5782.14 Å; $\chi_{ex}=1.64$ eV log gf (total) = -1.720 ^b		
Mn I	6013.4530	-0.7669	Cu I	5782.032	-3.4320
Mn I	6013.4740	-0.9790	Cu I	5782.042	-3.7349
Mn I	6013.4920	-1.2520	Cu I	5782.054	-3.0340
Mn I	6013.5010	-1.4561	Cu I	5782.064	-3.0850
Mn I	6013.5080	-1.6622	Cu I	5782.073	-3.3890
Mn I	6013.5130	-1.3100	Cu I	5782.084	-2.6880
Mn I	6013.5210	-1.3312	Cu I	5782.086	-3.0340
Mn I	6013.5270	-1.4861	Cu I	5782.098	-3.0340
Mn I	6013.5370	-1.8083	Cu I	5782.113	-2.6880
Mn I	6013.5410	-1.8541	Cu I	5782.124	-2.6880
Mn I	6013.5410	-2.4104	Cu I	5782.153	-2.5870
Mn I	6013.5420	-2.0302	Cu I	5782.173	-2.2410

Notes. log gf total sources: ^(a) NIST; ^(b) Bielski (1975)

3. Abundances

In the present work we derived the abundances based on a spectrum synthesis for 14 stars that were previously analyzed by Smiljanic et al. (2007). Although the focus of this paper is on performing relations between abundances of some iron peak and heavy elements, other elements than those discussed here are also shown in tables, in order to assemble all abundances determined so far for these stars in a single source, as explained in Sects. 3.1 and 3.3. Smiljanic and co-authors had already derived abundances for some of these elements through equivalent widths, but more accurate results are expected from spectrum synthesis both for heavy elements with weak and very strong lines. The abundance results line by line are shown in Table 2, and the average abundances are shown in Table 3. Abundances of Mn that were previously unpublished as well as new calculations for the abundance uncertainties for the 26 stars of Allen & Barbay (2006a) are also shown in Tables 2 and 3. Details of the sample, the atmospheric parameters, and the abundances derivation are described there.

Smiljanic et al. (2007) and Allen & Barbay (2006a) employ different methods to obtain the stellar atmospheric parameters T_{eff} , log g , [Fe/H] and microturbulence, so we needed to establish a satisfactory consistence between the two sets of parameters, essentially the T_{eff} scales. Smiljanic et al. (2007) rely on the excitation and ionization equilibria of Fe I/Fe II to derive the parameters self-consistently from the spectroscopic data alone, while Allen & Barbay (2006a) derive T_{eff} from photometry and the surface gravity from the stellar positions in the HR diagram. Allen & Barbay (2006a), however, also obtain excitation and ionization T_{eff} values, which agree well with the photometric ones. Also, Smiljanic et al. (2007) compare their spectroscopic surface gravities with those derived from the stellar positions in HR diagrams, and reported excellent agreement between the two surface gravity scales, except for HD 204075, which is the most massive and brightest star of their sample. We may then accept the sets of atmospheric parameters of these two works as consistent and can directly compare the abundances.

The LTE spectrum synthesis calculations were performed by employing the code by Spite (1967) and subsequent improvements in the past thirty years, which are described in Cayrel et al. (1991) and Barbay et al. (2003). The adopted model atmospheres (NMARCS) were computed with a version of the MARCS code, initially developed by Gustafsson et al. (1975) and subsequently updated by Plez et al. (1992). The usual notations $\log \epsilon(A) = \log(N_A/N_H)+12$ and $[A/B] = \log(N_A/N_B)_* - \log(N_A/N_B)_\odot$ were adopted, where N_A and N_B are the number abundances of species “A” and “B”, respectively. The sources of solar abundances are shown at the end of Table 3.

3.1. Light elements

Strong CH and CN bands are characteristics of barium stars, and these bands are stronger for giants than for dwarfs. Because they affect the blue region of the spectrum where many lines of heavy elements appear, it is very important to determine the C and N abundances before those of heavy elements, especially for giant stars. The spectrum synthesis of the heavy elements was carried out only after the C and N abundances were determined. Table 2 shows the lines used as reference for each relevant molecule, C₂, CH, and CN, to derive the average of C and N abundances for the sample stars, which we show in Table 3. One of the CN molecule transition suffers from a blend with some Li lines around $\lambda 6708$, and therefore we had to calculate the Li abundances. For the stars

of the present work, low Li abundances are expected given that all of them have already evolved to the red giant branch, where the Li depletion is considerable. The coolest star HD 220009 is the most Li-poor, with $T_{eff} = 4370\text{K}$ and $\log(\text{Li}) = -0.94$. These results agree with Fig. 4 of Allen & Barbuy (2006a).

Oxygen abundances were derived to be used below in a comparison with the abundances of elements produced by the r -process, since they are thought to share the same nucleosynthetic origin, massive stars. The forbidden lines at $\lambda 6300$ and $\lambda 6364$ were used, and the results are shown in Tables 2 and 3.

3.2. Iron-peak elements

For lines of Mn I, the hyperfine structure (hfs) was taken into account by employing a code made available by Andrew McWilliam following the calculations described by Prochaska et al. (2000). The hfs constants for Mn I were taken from Brodzinski et al. (1987) and Walther (1962). The nuclear spin ($I=2.5$) of the only nuclide that contributes to the manganese abundance (^{55}Mn) was found in Woodgate & Martin (1957). Table 4 shows the hfs components, excitation potential and adopted total $\log gf$ values with their references. Abundances derived from the five available lines of Mn usually agree well. All values of $[\text{Mn}/\text{Fe}]$ for the stars of the present work are below solar, as shown in Fig. 1. These low values for $[\text{Mn}/\text{Fe}]$ for $[\text{Fe}/\text{H}] < 0.0$ agree with the results of Feltzing et al. (2007) for disk stars.

For three lines of Cu I, the hfs from Biehl (1976) was taken into account, considering the isotopic fractions of 0.69 for ^{63}Cu and 0.31 for ^{65}Cu . In this case, small corrections were applied in a way that the total $\log gf$ values equal those of Bielski (1975) or the National Institute of Standards & Technology (NIST, Martin et al. 2002), which we adopt. The hfs components for Cu I lines are listed in Table 4. The lines for which hfs were used were checked using the solar (Kurucz et al. 1984) and Arcturus spectra (Hinkle et al. 2000). Similarly to the report of Allen & Barbuy (2006a), for some stars the line $\lambda 5218.2$ of Cu I results in higher abundances than $\lambda 5105.5$ and $\lambda 5782.1$.

Four lines of Zn I were used to compute the Zn abundances, and usually good agreement was secured for the abundances resulting from these lines. A difference ranging from 0.25 to 0.6 dex, usually between the $\lambda 4680.1$ and $\lambda 6362.3$ lines was observed for two stars of the present sample, and we note that a similar effect was also observed in six stars of the Allen & Barbuy 2006a sample.

As seen in Fig. 2, the abundances for Mn, Cu, and Zn of Smiljanic et al. (2007) are larger than in our work, the total $\log gf$ adopted by the former being the larger. We share four Mn I and two Cu I lines with Smiljanic et al. (2007). As they used larger $\log gf$, lower values for abundances would be expected, but the opposite occurred. This offset could be caused by the partially different line set, where ours is the more extensive. For Zn, Smiljanic et al. (2007) used only one line, whose $\log gf$ is 0.263 lower than ours. The differences between their Zn abundances and ours are around 0.3 dex, except for two stars, for which an agreement commensurate with the difference between the $\log gf$'s is found.

3.3. Neutron capture elements

In the present work we only discuss the correlations involving the abundances of Mn, Cu, and Zn with those of Sr, Y, Ba, Nd as representatives of the s -process, and Eu, Gd and Dy as rep-

resentatives of the r -process, because the nucleosynthetic production of Ba, Y, and Nd is highly dominated by the s -process by $\sim 81\%$, $\sim 92\%$ and $\sim 65\%$ respectively, whereas the r -process contributes with $\sim 94\%$ to the Eu and $\sim 85\%$ to the Gd and Dy production, according to Arlandini et al. (1999). A full analysis for Zr, Mo, Ru, La, Ce, Pr, Sm, Hf, Pb as well is postponed to a forthcoming paper. The abundance results for these elements confirm the preliminary abundance derivations from equivalent widths performed by Smiljanic et al. (2007), where the stars HD 13611, HD 20894, and HD 220009 were found to be normal instead of mild barium stars, given that the abundance of elements produced by s -process is much lower for these stars than for the other eight that could be called bona fide barium stars (see Table 3). The average abundances of Sr and Zr shown in Table 3 were computed only from the lines of Sr II and Zr II. The same hfs employed in Allen & Barbuy (2006a) was used for all lines of Ba, La, and Eu.

3.4. Uncertainties

Uncertainties on abundances were calculated by using an equation similar to Eq. 14 of Allen & Barbuy (2006a) or Eq. 1 of Allen & Porto de Mello (2007), but adding a term that takes care of the signal-to-noise (S/N) ratio. New uncertainties for the abundances found in Allen & Barbuy and Allen & Porto de Mello were derived with Eq. 1 and are given in Table 3 along with abundances and uncertainties for the elements studied here. In these derivations, we used the typical uncertainties on the atmospheric parameters determined by Allen & Barbuy, $\sigma_{T_{eff}} = 100\text{K}$, $\sigma_{[\text{Fe}/\text{H}]} = 0.04$ dex (if $\log g \geq 3.3$) or $\sigma_{[\text{Fe}/\text{H}]} = 0.18$ dex (if $\log g < 3.3$), $\sigma_{\log g} = 0.1$ dex, and $\sigma_{\xi} = 0.1$ km/s (see their Sect. 3.5), and those by Smiljanic et al. (2007), $\sigma_{T_{eff}} = 50$ K, $\sigma_{[\text{Fe}/\text{H}]} = 0.1$ dex, $\sigma_{\log g} = 0.35$ dex, and $\sigma_{\xi} = 0.06$ km/s (see Table 1).

Recalling that “ A_p ” is the output of the synthesis program, we have

$$\sigma_{A_p} = \sqrt{(\Delta A_T)^2 + (\Delta A_{mt})^2 + (\Delta A_l)^2 + (\Delta A_{\xi})^2 + (\Delta A_{sn})^2}, \quad (1)$$

where ΔA_T , ΔA_{mt} , ΔA_l , ΔA_{ξ} are the differences on A_p for each element because of variations of 1σ in the temperature, metallicity, $\log g$, and microturbulence velocity, respectively. The last term, ΔA_{sn} , is the difference on A_p after adding $(\text{S/N})^{-1}$ to the spectrum of the reference stars defined in Allen & Barbuy and Allen & Porto de Mello. The S/N ratios shown in Table 5 were measured in a window around $\lambda 6000$.

The variations on the abundances owing to the atmospheric parameters were computed for only one line, and we extended this result to all other lines of a given element. Indeed, the ideal procedure would be to compute all variations for all lines, since each line reacts differently to these variations, according to their atomic constants. This process entails synthesizing each line more than five times. This very time consuming approach does not compare favorably with a simpler procedure, when one considers the resulting very small improvement in accuracy. We were nevertheless very careful in the choice of the line employed for the uncertainty evaluation, to minimize the loss in accuracy by adopting the simpler procedure. The profile of the adopted line must be as well defined as possible, neither too strong nor too weak, and also affected by noise in an average way, to make the line useful.

By adopting this procedure, the larger the number of lines employed to derive the abundance of a given element, the lower the expected loss of accuracy. Thus, n in Eq. 15 of

Table 5. Signal to noise measured around $\lambda 6000$ for stars analyzed here and in Allen & Barbuy (2006a).

Star	SN	Star	SN	Star	SN	Star	SN
HD 749	220	HD 26967*	180	HD 107574	230	HD 188985	150
HD 2454	210	HD 27271	220	HD 113226*	330	HD 202109	190
HD 5424	150	HD 46407	160	HD 116713	110	HD 204075	320
HD 8270	230	HD 48565	220	HD 116869	190	HD 205011	210
HD 9362*	310	HD 76225	140	HD 123396	200	HD 210709	170
HD 12392	180	HD 87080	200	HD 123585	100	HD 210910	260
HD 13551	190	HD 89948	370	HD 139195	420	HD 220009*	390
HD 13611*	370	HD 92545	140	HD 147609	150	HD 222349	130
HD 20894*	440	HD 104979	140	HD 150862	180	BD+18 5215	100
HD 22589	190	HD 106191	110	HD 181053	240	HD 223938	360

Allen & Barbuy is the number of lines used to compute the average of the abundance for each element for each star, shown in their Table 15.

3.5. Abundance scatter

Abundance ratios from our sample and stars from the literature are shown in Figs. 1 and 3 - 8. In general, the $[\text{Mn}/\text{Fe}]$ derived by us follows the trend found in the literature, except for the high values of some stars from Luck & Bond (1991) and Smith et al. (1993). The stars with the lowest values for $[\text{Cu}/\text{Fe}]$ in Fig. 1 are those with metallicities and kinematics characteristic of the halo, with $[\text{Fe}/\text{H}] < -1$. Some of these stars, indicated with a big open square in Figs. 1, 3, 4, 5, and 8, figure in Mennessier et al. (1997)'s work, and were classified by them as belonging to the halo population through kinematical criteria. It is worthwhile to note, however, that the abundance patterns of some of these stars do not match Mennessier et al.'s kinematical criteria. Furthermore, the $[\text{Cu}/\text{Fe}]$ value of He2-467 seems too low to be explained away by membership in the halo population of the Galaxy, whereas some stars from Smith et al. (1993) have $[\text{Cu}/\text{Fe}]$ too high for disk stars. Yet $[\text{Zn}/\text{Fe}]$ from all works in Fig. 1 follows the trend found in the literature in this range of metallicities.

High scatter may prevent accurate conclusions about abundance trends. Some degree of scatter is always expected, but the origin of such a high degree of scatter as seen in Fig. 1 for Mn abundances is elusive. Intrinsic cosmic scatter can be the result of the heterogenous nature of the original interstellar medium from which each star was formed. However, all too often scatter arises from differences in the procedure used by different authors, which could involve parameters as diverse as different line sets, atomic constants, hfs employed (del Peloso et al. 2005), solar abundances as reference, atmosphere models, and spectral synthesis codes.

Table 6 shows that the difference between results obtained for Mn abundances by different authors for some stars can reach 0.50 dex, whereas for Cu and Zn this difference is smaller. For these eight stars, only the abundances from this work and Allen & Barbuy (2006a) are shown in figures. The different values for $\log gf$ adopted by different authors might be one of the main sources of the scatter in the abundance ratios, since an increase of a certain amount in the $\log gf$ results in a reduction of approximately the same amount in the abundance (Gray 1992). We thus preferred to use in the fits only the abundances from the literature derived from the laboratory $\log gfs$. Yet, this cannot allow a conclusion as to why the anticorrelation suggested by Castro et al. (1999) between $[\text{Cu}/\text{Fe}]$ and $[\text{Ba}/\text{Fe}]$ is not verified in our analysis (Fig. 3), but we note that the abundance inter-

val considered here is larger than in Castro et al. (1999), and our conclusions consequently more robust.

Considering the binary scenario for the origin of stars that show enhanced s -process elements, and their appearance in any galactic population, one might suggest that the origin of at least part of the scatter in the case of s -process enriched stars could reside in the different composition of the material dredged up to the surface of the former primary component and transferred onto the secondary component. This is supported by Figs. 3 - 5, where the scatter seems to be larger when the Mn, Cu, and Zn abundances are related to those of an element with a larger contribution of the s -process for its formation, namely Ba, Y, and Nd, while an apparent low scatter is found when the abundances are related to those of the r -process elements, Eu, Gd, and Dy. We note, however, that data for Eu, Gd, and Dy are much scarcer in the literature compared to Ba, Y, and Nd, which are more widely studied and are therefore more likely to involve differences in method. Indeed, we employed for Dy only data from Allen & Barbuy (2006a) and our work, which both employ the same atomic data and spectral synthesis routine.

The main s -processing strongly depends on the initial mass of the AGB star (see e.g. Bisterzo et al. 2010). A TP-AGB with low initial mass suffers less third dredge-up episodes than stars with higher masses (e.g. Lugaro et al. 2003; Bisterzo et al. 2010). Therefore, the degree of enrichment in carbon and heavy elements of the barium star depends on the initial mass of the companion white dwarf. Chen et al. (2003, and references therein) studied how to recover the initial mass of the white dwarf in binary systems.

Furthermore, the transfer of enriched gas from the AGB star to the pre-barium star depends on their masses and the binary separation. Because the AGB star wind is generally much stronger than that of the pre-barium star, the wind of the latter is usually neglected in the calculations of mass-loss/accretion rate through winds in binary systems (Han et al. 1995). The higher the AGB mass, the larger its mass-loss rate and the higher its wind velocity. A dependence of the wind velocity of the primary star on its radius and the binary separation is given by de Kool & Green (1995). High AGB wind velocities result in lower mass accretion rate by the pre-barium star. On the other hand, the mass accretion rate undergone by the pre-barium star directly depends on its mass. A large separation of the two components of the binary system results in a higher wind velocity that reduces the mass accretion rate of the pre-barium star.

4. Discussion

Castro et al. (1999) have suggested an anticorrelation between $[\text{Cu}/\text{Fe}]$ and $[\text{Ba}/\text{Fe}]$ for a sample of solar-type disk stars, including stars from the young, solar-metallicity Ursa Major kinematical group: this anticorrelation was proposed before by Pereira & Porto de Mello (1997) and Pereira et al. (1998) for two Ba-enriched symbiotic stars. The $[\text{Cu}/\text{Fe}]$ vs. $[\text{Ba}/\text{Fe}]$ run including stellar abundances of the present work and others selected from the literature shows no evidence of such an anticorrelation, as can be clearly seen in Fig. 3b. The pattern seen in Fig. 6 of Castro et al. can indeed be seen in our Fig. 3b, but only by isolating the data used in their plot. Indeed, their results along with ours and those of Allen & Barbuy (2006a) essentially follow a flat trend. With the aim to more extensively investigate this suspected anticorrelation, we included other iron peak elements (Mn and Zn) and verified their behavior as it relates to Ba and other s - and r -elements.

4.1. Relations with heavy elements

In order to evaluate the correlations between iron peak and neutron capture elements, least-square fits were performed considering the uncertainties provided by the authors of the corresponding abundance analysis, the results of which we show in Table 7. For all fits the covariance is around zero, indicating that the two variables involved may be independent. If both ratios are below or above the expected value, the covariance is positive. When one ratio is above and the other is below the expected value, the covariance is negative.

For the fits we considered only the barium stars analyzed here, Allen & Barbuy (2006a) and one star of Pereira & Junqueira (2003). The same stars were used in the fits involving Eu in Fig. 4. This is indicated in the labels of Figs. 3 and 4.

The correlation with Dy is expectedly poor owing to the low number of available lines of this element. For the star HD 5424 the Dy abundance is unusually high, $(\text{Dy}/\text{Fe}) = 1.65$, (see Allen & Barbuy 2006a). A higher Dy abundance for barium stars is expected because this element is in the *s*-process path, but an abundance as high as this is probably suspect. However, the χ_{red}^2 for $[\text{Cu}/\text{Fe}]$ vs $[\text{Dy}/\text{Fe}]$ in Fig. 5 is very close to 1, indicating the good quality of the fit, even if the HD 5424 data point is kept.

The runs involving $[\text{Mn}/\text{Fe}]$ show very weak correlations and low quality in the fits, with $\chi_{red}^2 \sim 2.4$. The large scatter clearly prevents better fits as well as a more definitive conclusion. The absent correlation of $[\text{Mn}/\text{Fe}]$ with the *r*-element abundances is not compatible with a significant production of Mn in SN II. Similarly, the lack of correlation with the *s*-element abundances indicates that the bulk of the Mn production is very probably not taking place in AGB stars. This indicates that the production of Mn is a mix of several processes.

Indeed, several works have proposed quite diverse sites for the nucleosynthesis of Mn. Gratton (1989) attributed the significant increase of $[\text{Mn}/\text{Fe}]$ for $[\text{Fe}/\text{H}] > -1$ to an overproduction of Mn by SN Ia, whereas McWilliam et al. (2003) suggested that this effect could be a result of metallicity-dependent yields of Mn in both SN Ia and SN II (e.g. Arnett 1971; Woosley & Weaver 1995; Chieffi & Limongi 2004; Limongi & Chieffi 2005). The Mn yields of SN II would increase as more metal-rich progenitors produce higher amounts of Mn, producing the increasing $[\text{Mn}/\text{Fe}]$ trend already seen by Gratton (1989). Regarding the *s*-process, the weak component could eventually contribute to the production of Mn, because this component acts for nuclei with $A < 56$, whereas no significant contribution is expected from the main component for this region of atomic mass. The behavior of Mn with these components is discussed in Sect. 4.3. Our results therefore support an interpretation in which the bulk of the Mn production originates in SN Ia.

The runs of $[\text{Cu}/\text{Fe}]$ vs. $[\text{Ba}, \text{Y}, \text{Nd}/\text{Fe}]$ show a slightly increasing trend, even though the slope of the relation with Ba and Y is clearly of little significance. We found no trend for Nd. The runs of $[\text{Cu}/\text{Fe}]$ vs. $[\text{Eu}/\text{Fe}]$ also show a slightly increasing trend with much lower scatter compared to the *s*-process elements. Particularly, the runs of $[\text{Cu}/\text{Fe}]$ with $[\text{Gd}, \text{Dy}/\text{Fe}]$ are fairly tight and essentially flat. The weak correlation between Cu and the *r*-elements indicates that the bulk of the Cu production does not come from SN II. According to the Mishenina et al. (2002) estimate, the bulk of the Cu abundance (~ 62 -65%) should be owed to SN Ia, in agreement with Matteucci et al. (1993), 25% to a secondary process in massive stars and only a small fraction (7-8%) to a primary process. A similar result was obtained by Cunha et al. (2002) for the ω Cen globular cluster, where these

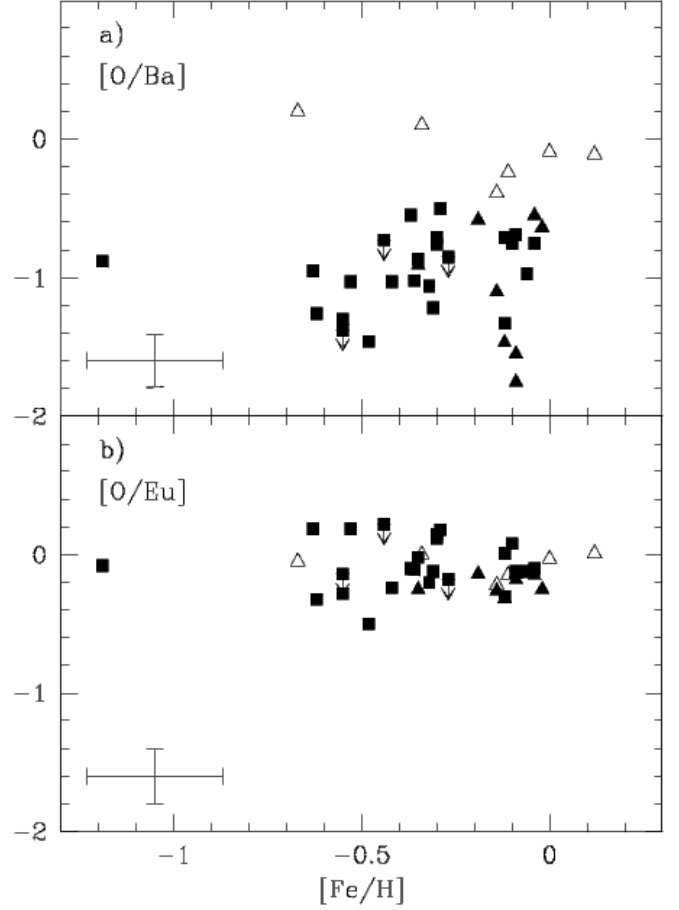


Fig. 6. $[\text{O}/\text{Ba}]$ and $[\text{O}/\text{Eu}]$ vs. $[\text{Fe}/\text{H}]$. Symbols are the same as in Fig. 7. Error bars are defined as in Fig. 1.

authors conclude that the *r*-process contribution to the synthesis of Cu must be low. Our result is thus in line with previous literature results, which indicate a low contribution of SN II to the synthesis of Cu.

The $[\text{Zn}/\text{Fe}]$ vs. $[\text{Ba}, \text{Y}, \text{Nd}/\text{Fe}]$ runs show a clearly increasing trend with statistically significant correlations. The runs of $[\text{Zn}/\text{Fe}]$ vs. $[\text{Eu}/\text{Fe}]$ show an increasing trend with much lower scatter when compared to the $[\text{Zn}/\text{Fe}]$ vs. $[\text{Ba}, \text{Nd}, \text{Y}/\text{Fe}]$ plots, and the correlation due to Zn is stronger than in the case of Cu. $[\text{Zn}/\text{Fe}]$ increases much faster than $[\text{Cu}/\text{Fe}]$ with $[\text{Eu}, \text{Gd}, \text{Dy}/\text{Fe}]$. This result suggests that for Zn a higher abundance fraction is owed to *r*-process than for Cu. Mishenina et al. (2002) concluded that $\sim 30\%$ of the synthesis of Zn would be owing to a primary source acting in massive stars, similarly to Fe, $\sim 67\%$ would originate in SN Ia and only $\sim 3\%$ of the abundance of Zn could be owing to AGB stars. The stronger correlation between Zn and *r*-elements agrees with the conclusion that the contribution of the *r*-process is more significant for Zn than for Cu.

4.2. Production of iron peak elements in SN II

Recently, Feltzing et al. (2007) obtained the run of $[\text{Mn}/\text{O}]$ against $[\text{O}/\text{H}]$ in an attempt to better separate the contributions of SN Ia and SN II to the synthesis of Mn, because oxygen is a virtually exclusive product of SN II, while the Fe yield has contributions from both types of SN (Timmes et al. 1995). This interpretation is well confirmed by the behavior of oxygen when related to europium in our sample stars, as shown in Fig. 6: re-

garding [O/Eu] vs. [Fe/H], barium and normal stars are mixed and the scatter is smaller than in the [O/Ba] vs. [Fe/H] plot, where barium and normal stars are clearly segregated. As Eu and O are believed to be released to the interstellar medium in the same class of event, type II SNe, a flat [O/Eu] vs. [Fe/H] is expected. Yet, considering barium, an *s*-element, there is no clear correlation between [O/Ba] and [Fe/H]. Note that the normal stars lie above all other data because their Ba abundances are much lower when compared to the barium stars, while the abundance of O is the same for both. Whereas the [Mn,Cu/O] vs. [O/H] runs in our Fig. 7 are essentially flat, [Zn/Fe] vs. [O/H] shows a clearly decreasing trend.

Figure 13 of Feltzing et al. (2007) shows that the run of [Mn/O] vs. [O/H] is flat up to [O/H] = -0.5 for halo and metal-poor thick-disk stars, indicating that the yields of Mn and O are well balanced in this interval. For [O/H] ≥ -0.5, [Mn/O] vs. [O/H] shows an increasing trend. According to Bensby et al. (2004), the archetypal signature of SN Ia in the thick disk does not occur up to [O/H] = 0, so this increasing trend could be attributed to metallicity dependent Mn yields in SN II, the SN Ia contributing to the synthesis of Mn only later. However, they also concede that the contribution of SN Ia to the rise of Mn in the thin disk cannot be completely neglected. The increasing trend of [Mn/O] vs. [O/H] as shown in Fig. 13 of Feltzing et al. (2007) for [O/H] ≥ -0.5 is not seen in our Fig. 7, even considering that most of our stars belong to the disk, according to Mennessier et al. (1997). Therefore, if one accepts that the nucleosynthetic disk signature of SN Ia does not occur before [O/H] = 0, the decrease of [Zn/O] in our Fig. 7 could be more directly interpreted as caused by the action of metallicity-dependent yields in massive stars between these two elements, and concurring with our previous conclusion that a larger fraction of the synthesis of Zn is owed to massive stars than is the case for Cu.

Concerning Mn, the previous absence of correlation between [Mn/Fe] and the *r*-process elements in our Fig. 5 and Fig. 4, along with the flat [Mn/O] vs. [O/H] (Fig. 7), again strengthens the interpretation that little is owed to massive stars in the synthesis of Mn, again attributing the bulk of the synthesis of oxygen and the *r*-process elements to massive stars. Most of the Mn synthesis would then be due to SN Ia, in line with the views of Nissen et al. (2000) and Carretta et al. (2004).

4.3. Main and weak *s*-components

Given that Mn, Cu, and Zn are thought to be partly produced by the weak component of the *s*-process, and Sr also has an important contribution from this component (Lugaro et al. 2003), we also investigated how the abundances of all these elements are related. At first we created [Mn,Cu,Zn/Fe] vs. [Sr/Fe] plots as shown in panels a), b), and c) of Fig. 8. [Mn/Fe] vs. [Sr/Fe] seems to have a flat trend, while [Cu/Fe] vs. [Sr/Fe] yields an increasing trend, which is even stronger for [Zn/Fe] vs. [Sr/Fe]. Next, we related the abundances of Mn, Cu, and Zn (log ϵ) to the logarithm of the abundance fraction correspondent to the weak component of the *s*-process for Sr, as shown in panels d), e), and f) of Fig. 8. For the stars of our work, the separation of the abundances according to the nucleosynthetic process was made as in Allen & Barbuy (2006b), and the values will be shown in a forthcoming paper. The values of χ_{red}^2 shown in Table 7, as well as the uncertainties in the correlation coefficients, tell us that there are increasing and statistically significant correlations, confirming that significant fractions of Mn, Cu, and Zn are produced by the weak component of the *s*-process. In this case, the

normal stars can be included given that there is no difference in the separation of components for both normal and barium stars.

To investigate how the abundances of Mn, Cu, and Zn are related to the abundance fraction corresponding to the main component of the *s*-process (Allen & Barbuy 2006b) we have added panels g), h), and i) of Fig. 8. Normal stars were obviously excluded from these panels. If Cu was preferentially depleted to produce Ba through the main component of the *s*-process we would see a decreasing trend, but the opposite is seen instead. That the [Cu/Fe] ratio is mostly flat when related to neutron capture elements indicates that Cu is little, if at all, affected by the *s*-process in the possible role of a seed nucleus. On the other hand, considering the *s*-process as a chain starting in ^{56}Fe and ending in Bi, Cu is also in the *s*-process path, so it is produced as well as destroyed, and our results suggest that it is being preserved after all. A very similar effect is seen for Zn. Our results agree well with the assertion by Matteucci et al. (1993) that only a very low contribution of the main component of the *s*-process goes to the abundances of Zn and Cu, whereas the contribution of the weak component is higher.

Lastly, it still stands out in the case of Cu that the two aforementioned metal-poor, yellow symbiotic stars of the halo, Hen 2-467 and BD-21°3873 analyzed by Pereira et al. (1998) and Pereira & Porto de Mello (1997), respectively, do present a very low [Cu/Fe] ratio that remains unexplained. Perhaps these objects have something interesting to reveal about the operation of the *s*-process operating in a regime different from most Ba-rich stars discussed here.

5. Conclusions

We presented previously unpublished Mn abundances based on spectrum synthesis for the barium star sample of Allen & Barbuy (2006a) and new C, N, O, Mn, Cu, Zn and heavy element abundances for the barium star sample of Smiljanic et al. (2007). Because barium stars show high overabundances in C and N, abundances for these elements were also derived before those of the heavy elements, because their lines are often affected by molecular bands of CH and CN.

We were able to clearly establish in our analysis that the stars considered to be normal by Smiljanic et al. (2007) show very low abundances of the *s*-elements when compared to bona fide barium stars, while this difference is much reduced for the *r*-elements. This confirms the previous analysis that these stars are normal instead of barium stars, which further indicates that additional work on proposed barium stars, that are classified based on old data is necessary in order to check whether they indeed belong to this class.

The [Mn,Cu,Zn/Fe] abundance ratios were correlated to elements that are nucleosynthetically dominated by the *s*-process (Ba, Y, Nd) and the *r*-process (Eu, Gd, Dy). The runs of [Mn/Fe] vs. [*s*-,*r*-elements/Fe] show much weaker correlations when compared to those of [Cu,Zn/Fe] vs. [*s*-,*r*-elements/Fe]. The absent correlation of [Mn/Fe] with the *r*- and *s*-element abundances along with the flat [Mn/O] vs. [O/H] indicate that the production of Mn is a mix of several processes, likely to be dominated by SN Ia nucleosynthesis, which agrees well with other works in the literature. The weak correlation between Cu and the *r*-elements indicates that the bulk of Cu production does not come from SN II. The increasing trend of [Zn/Fe] vs. [Eu/Fe] indicates that for Zn a higher abundance fraction is owed to massive stars than in the case of Cu.

Our results suggest that significant fractions of Mn, Cu, and Zn are produced by the weak component of the *s*-process based

on the increasing correlations found for Mn, Cu, and Zn abundances and the abundance fraction due to this process to the Sr abundance. On the other hand, the near absence of correlation between Mn, Cu, and Zn abundances and the abundance fraction of Ba due to the main component of the *s*-process suggests that only a very low contribution of this component goes to the abundances of Mn, Zn, and Cu. We found in particular that relations between the [Cu/Fe] ratio and those owed to neutron capture elements are mostly flat, suggesting that Cu is little if at all affected by the *s*-process in the possible role of a seed nucleus. This could indicate that Mn, Cu, and Zn are essentially preserved during the main *s*-processing in AGB stars. Our results point toward a significant contribution of the weak *s*-processing to the nucleosynthesis of Mn, Cu, and Zn.

Nevertheless, the complex behavior of the abundances of these elements remain unaccounted for by theoretical methods in its details. More abundance data, both for normal and chemically peculiar objects, would certainly contribute toward a better understanding of the nucleosynthesis of the elements in the transition region between the Fe-peak and neutron capture species.

Acknowledgements. DMA acknowledges the following post-doctoral fellowships: FAPERJ n° 152.680/2004, CAPES n° BEX 3448/06-1, and FAPESP n° 2008/01265-0. The STRI at the University of Hertfordshire, where part of this work was completed, is acknowledged by DMA. GFPM acknowledges financial support by CNPq grant n° 476909/2006-6, FAPERJ grant n° APQ1/26/170.687/2004, and a CAPES post-doctoral fellowship n° BEX 4261/07-0. We are grateful to Lício da Silva and Beatriz Barbuy for making available some of the spectra, and to Beatriz Barbuy for making available the spectrum synthesis code. We are also grateful for valuable suggestions from an anonymous referee and to Marcelo Porto Allen for his useful comments. Use was made of the Simbad database, operated at CDS, Strasbourg, France, and of NASA's Astrophysics Data System Bibliographic Services.

References

- Allende Prieto, C., Lambert, D.L., Asplund, M. 2001, *ApJ* 556, L63
 Allen, D.M., Barbuy, B. 2006a, *A&A*, 454, 895
 Allen, D.M., Barbuy, B. 2006b, *A&A*, 454, 917
 Allen, D.M., Porto de Mello, G.F. 2007, *A&A*, 474, 221
 Arlandini, C., Käppeler, F., Wisshak, K. 1999 *ApJ*, 525, 886
 Arnett, W.D. 1971, *ApJ*, 166, 153
 Barbuy, B., Perrin, M.-N., Katz, D., Coelho, P., Cayrel, R., Spite, M., Van't Veer-Menneret, C. 2003, *A&A*, 404, 661
 Barbuy, B., Renzini, A., Ortolani, S., Bica, E., Guarnieri, M.D. 1999, *A&A*, 341, 539
 Bensby, T., Feltzing, S., Lundström, I. 2004, *A&A*, 415, 155
 Bergstrom H., Biémont E., Lundberg H., Persson A., 1988, *A&A*, 192, 337
 Biehl, D. 1976, Ph.D. Thesis, Kiel University
 Bielski, A. 1975, *JQSRT*, 15, 463
 Biémont, E., Gamir, H.P., Palmeri, P., Li, Z.S., Svanberg, S. 2000, *MNRAS*, 312, 116
 Biémont E., Godefroid M. 1980, *A&A*, 84, 361
 Biémont, E., Grevesse N., Hannaford, P., Lowe, R.M., 1981, *ApJ*, 248, 867
 Biémont, E., Grevesse, N., Hannaford, P., Lowe, R.M. 1989, *A&A*, 222, 307
 Biémont, E., Lowe, R.M. 1993, *A&A*, 273, 665
 Bisterzo, S., Gallino, R., Straniero, O., Cristallo, S., Käppeler, F. 2010, *MNRAS*, 404, 1529
 Brodzinski T., Kronfeldt H.-D., Kropp J.-R., Winkler R., Z. 1987, *Phys. D*, 7, 161
 Carretta, E., Gratton, R.G., Gragaglia, A., Bonifacio, P., Pasquini, L. 2004, *A&A*, 416, 925
 Castro S., Porto de Mello G.F., da Silva L. 1999, *MNRAS*, 305, 693
 Cayrel, R., Perrin, M.N., Barbuy, B., Buser, R. 1991, *A&A*, 247, 108
 Chen, X., Han, Z. 2003, *MNRAS*, 341, 662
 Chieffi, A., Limongi, M. 2004, *ApJ*, 608, 405
 Corliss, C.H., Bozman, W.R., 1962, *Experimental Transition Probabilities for Spectral Lines of Seventy Elements (NBS Monograph 32)* (Washington: GPO)
 de Kool, M., Green, P.J. 1995, *ApJ*, 449, 236
 del Peloso, E. F., da Silva, L., Cunha, K. & Porto de Mello, G. F. 2005, *A&A*, 441, 1149
 Cunha, K., Smith, V.V., Suntzeff, N.B., Norris, J.E., da Costa, G.S. and Plez, B. 2002, *ApJ*, 124, 379
 Feltzing, S., Fohlman, M., Bensby, T. 2007, *A&A*, 467, 665
 Goly A., Kusz J., Nguyen Quang B., Weniger S., 1991, *JQSRT*, 45, 157
 Gratton, R.G. 1989, *A&A*, 208, 171
 Gratton, R.G., Sneden, C. 1991, *A&A*, 241, 501
 Gratton R.G., Sneden C., 1994, *A&A*, 287, 927
 Gray D.F. 1992 in *The observation and analysis of stellar photospheres*, Cambridge
 Grevesse, N., Sauval, A.J. 1998, *Space Sci. Rev.*, 85, 161
 Gustafsson, B., Bell, K.A., Eriksson, K., Nordlund, Å. 1975, *A&A*, 42, 407
 Han, Z., Eggleton, P.P., Podsiadlowski, P., Tout, C.A. 1995, *MNRAS*, 277, 1443
 Hannaford P., Lowe R.M., 1983, *Opt. Eng.*, 22, 532
 Hannaford P., Lowe R.M., Grevesse N., Biémont E., Whaling W., 1982, *ApJ*, 261, 736
 Hartog, E.A.D., Lawler, J.E., Sneden, C., Cowan, J.J. 2003, *ApJS*, 148, 543
 Hinkle, K., Wallace, L., Valenti, J., & Harmer, D. 2000, *Visible and Near Infrared Atlas of the Arcturus Spectrum 3727-9300 Å*, ed. K. Hinkle, L. Wallace, J. Valenti, and D. Harmer (San Francisco: ASP)
 Junqueira S., Pereira C.B. 2001, *AJ*, 122, 360
 Käppeler F., Beer H., Wisshak K., 1989, *Rep.Prog.Phys.*, 52, 945
 Kaufer, A., Stahl, O., Tubbesing, S., et al. 2000, *Proc. SPIE*, 1008, 459
 Kurucz, R. L., Furenlid, I., Brault, J. 1984, *Solar flux atlas from 296 to 1300 nm*, National Solar Observatory Atlas, Sunspot (New Mexico: National Solar Observatory)
 Kusz, J., 1992, *A&AS*, 92, 517
 Lage, C.S., Whaling, W. 1976, *JQSRT*, 16, 537
 Lamb, S.A., Howard, W.M., Truran, J.W., Iben, I.Jr. 1977, *ApJ*, 217, 213
 Lambert D.L., 1978, *MNRAS*, 182, 249
 Lawler, J.E., Bonvallet, G., Sneden, C. 2001a, *ApJ*, 556, 452
 Lawler, J.E., Wickcliffe, M.E., Hartog, A.D. 2001b, *ApJ*, 563, 1075
 Limongi, M., Chieffi, A. 2005, *ASPC*, 342, 122
 Luck R.E., Bond H.E. 1991, *ApJS*, 77, 515
 Lugaro, M., Davis, A.M., Gallino, R., Pellin, M.J., Straniero, O., Käppeler, F. 2003, *ApJ*, 593, 486
 Maier R.S., Whaling W., 1977, *JQSRT*, 18, 501
 Martin, W.C., Fuhr, J.R., Kelleher, D.E., et al. 2002, *NIST Atomic Database (version 2.0)*, <http://physics.nist.gov/asd>. National Institute of Standards and Technology, Gaithersburg, MD.
 Matteucci, F., Raiteri, C.M., Busso, M., Gallino, R., Gratton, R. 1993, *A&A*, 272, 421
 McClure, R. D., Fletcher, J. M., & Nemeç, J. M. 1980, *ApJ*, 238, L35
 McWilliam A., 1998, *AJ*, 115, 1640
 McWilliam, A., Rich, R.M. 1994, *ApJS*, 91, 749
 McWilliam, A., Rich, R.M., Smecker-Hane, T.A. 2003, *ApJ*, 592, L21
 Mennessier, M.O., Luri, X., Figueras, F., Gómez, A.E., Grenier, S., Torra, J., North, P. 1997, *A&A*, 326, 722
 Mishenina, T.V., Kovtyukh, V.V., Soubiran, C., Travaglio, C., Busso, M. 2002, *A&A*, 396, 189
 Nissen, P.E., Chen, Y.Q., Schuster, W.J., Zhao, G. 2000, *A&A*, 353, 722
 Palmeri, P., Quinet, P., Wyart, J.F., Biémont, E. 2000, *PhysS*, 61, 323
 Pereira C.B. 2005, *AJ*, 129, 2469
 Pereira C.B., Junqueira S. 2003, *A&A*, 402, 1061
 Pereira C.B., Porto de Mello G.F. 1997, *AJ*, 114, 2128
 Pereira C.B., Smith V.V., Cunha K. 1998, *AJ*, 116, 1977
 Plez, B., Brett, J.M., Nordlund, A. 1992, *A&A*, 256, 551
 Prochaska, J.X., Naumov, S.O., Carney, B.W., McWilliam, A., Wolfe, A.M. 2000, *AJ*, 120, 2513
 Raiteri, C.M., Gallino, R., Busso, M., Neuberger, D., Käppeler, F. 1993, *ApJ*, 419, 207
 Rutten R.J., 1978, *SoPh*, 56, 237
 Smiljanic, R., Porto de Mello, G.F., da Silva, L. 2007, *A&A*, 468, 679
 Smith, V.V., Suntzeff, N.B., Cunha, K., Gallino, R., Busso, M., Lambert, D.L., Straniero, O., 2000, *AJ*, 119, 1239
 Smith, V.V., Coleman, H., Lambert, D.L. 1993, *ApJ*, 417, 287
 Sneden, C., Gratton, R.G., Crocker, D.A. 1991, *A&A*, 246, 354
 Sneden C., McWilliam A., Preston G.W., et al., 1996, *ApJ*, 467, 819
 Spite, M. 1967, *Ann.. Astrophys.* 30, 211
 Thévenin, F., 1989, *A&AS*, 77, 137
 Thévenin, F., 1990, *A&AS*, 82, 179
 Timmes, F.X., Woosley, S.E., Weaver, T.E. 1995, *ApJS*, 98, 617
 Walther, H. 1962, *Z. Phys.*, 170, 507
 Woodgate, G.K., Martin, J.S. 1957, *Proc. Phys. Soc. Lon. A*, 70, 485
 Woosley, S.E., Weaver, T.A. 1995, *ApJS*, 101, 181
 Yushchenko, A.V., Gopka, V.F., Kim, C., Liang, Y.C., Musae, F.A., Galazutdinov, G.A. 2004, *A&A*, 413, 1105

Table 1. Stellar parameters for the sample stars derived by Smiljanic et al. (2007). T_{exc} : excitation temperature; $\log g$: surface gravity; $[Fe/H]$: metallicities; ξ : microturbulent velocities; BC(V): bolometric correction; M_v : absolute magnitudes; M_{bol} : bolometric magnitude; L_*/L_\odot : luminosities; M_*/M_\odot : masses. Numbers in parenthesis are errors in last decimals.

Star	T_{exc} (K)	$\log g$ (cgs)	$[Fe/H]$	ξ (km/s)	BC(V)	M_v	M_{bol}	L_*/L_\odot	M_*/M_\odot
HD 9362	4780(50)	2.43(35)	-0.34(7)	1.71(6)	-0.34	+0.78	+0.44(4)	1.75(2)	1.9
HD 13611	5120(50)	2.49(35)	-0.14(6)	1.96(6)	-0.22	-0.76	-0.98(21)	2.35(9)	3.6
HD 20894	5080(50)	2.60(35)	-0.11(6)	1.80(6)	-0.23	+0.04	-0.19(14)	2.00(5)	3.0
HD 26967	4650(50)	2.51(35)	0.00(7)	1.52(6)	-0.39	+1.21	-0.81(3)	1.60(1)	1.5
HD 46407	4940(50)	2.65(35)	-0.09(12)	1.87(6)	-0.28	+0.97	+0.68(16)	1.65(7)	2.3
HD 104979	4920(50)	2.58(35)	-0.35(5)	1.71(6)	-0.29	+0.63	+0.34(6)	1.79(3)	2.3
HD 113226	5082(50)	2.85(35)	+0.12	1.86(6)	-0.23	+0.47	+0.24(4)	1.83(2)	2.9
HD 116713	4790(50)	2.67(35)	-0.12(13)	1.97(6)	-0.34	+1.23	+0.89(8)	1.57(3)	1.9
HD 139195	5010(50)	2.89(35)	-0.02(6)	1.67(6)	-0.26	+1.07	+0.82(9)	1.60(4)	2.4
HD 181053	4810(50)	2.48(35)	-0.19(6)	1.70(6)	-0.33	+0.64	+0.31(21)	1.80(8)	2.2
HD 202109	4910(50)	2.41(35)	-0.04(7)	1.85(6)	-0.29	-0.01	-0.31(3)	2.05(1)	3.0
HD 204075	5250(50)	1.53(35)	-0.09(12)	2.49(6)	-0.18	-1.57	-1.76(18)	2.63(7)	4.2
HD 205011	4780(50)	2.41(35)	-0.14(9)	1.70(6)	-0.34	+0.54	+0.20(15)	1.85(6)	2.2
HD 220009	4370(50)	1.91(35)	-0.67(7)	1.61(6)	-0.52	+0.11	-0.41(13)	2.09(5)	1.0

Table 6. Data from the literature for stars that were analyzed in more than one work.

Star	Ref	$[Fe/H]$	$[Mn/Fe]$	$[Cu/Fe]$	$[Zn/Fe]$	$[Y/Fe]$	$[Ba/Fe]$	$[Nd/Fe]$	$[Eu/Fe]$	$[Gd/Fe]$	$[Dy/Fe]$
HD 8270	1	-0.42	-0.29	-0.21	-0.04	0.95	1.11	0.73	0.32	0.25	0.04
HD 8270	2	-0.53	-0.07	-0.07	0.04	0.75	1.17	0.80	0.19
HD 13551	1	-0.44	-0.30	-0.17	0.10	1.08	1.16	0.73	0.21	0.55	0.09
HD 13551	2	-0.28	-0.22	0.03	0.04	0.90	1.38	0.53
HD 22589	1	-0.27	-0.10	0.00	0.11	0.83	0.88	0.32	0.21	0.03	0.04
HD 22589	2	-0.16	0.16	0.06	0.06	0.72	0.75	0.07	0.26
HD 87080	1	-0.44	-0.31	-0.25	0.10	1.11	1.48	1.56	0.66	0.90	1.14
HD 87080	3	-0.51	-0.09	0.01	0.26	1.01	1.51	0.97	0.61
HD 89948	1	-0.30	-0.17	-0.17	0.02	1.02	0.99	0.65	0.16	0.25	-0.31
HD 89948	4	-0.27	0.18	0.08	...	1.11	0.83	0.60
HD 89948	5	-0.12	-0.32	...	-0.24	0.85	0.86	0.59
HD 123585	1	-0.48	-0.30	0.04	0.10	1.34	1.79	1.41	0.83	0.55	0.64
HD 123585	5	-0.50	1.14	1.32	0.98
HD 150862	1	-0.10	-0.14	-0.12	0.00	1.08	1.03	0.34	0.20	0.23	0.14
HD 150862	5	-0.22	0.22	...	-0.25	0.65	...	0.32
HD 202109	6	-0.04	-0.35	-0.17	-0.22	0.44	0.57	0.18	0.17	0.06	-0.05
HD 202109	7	0.01	-0.25	-0.01	-0.08	0.48	...	0.42	0.32	...	0.33

References. (1) Allen & Barbuy (2006a); (2) Pereira (2005); (3) Pereira & Junqueira (2003); (4) Smith et al. (1993); (5) Luck & Bond (1991); (6) This; (7) Yushchenko et al. (2004).

Table 7. Results of the least-squares fits for Figs. 3, 4, 5, and 8. “Cov” is the covariance between “A” and “B” for the linear fit $Y(X) = AX + B$ (first column), and “D.O.F.” is the number of degrees of freedom.

Least-squares fits for Fig. 3			
$Y(X) = AX + B$	χ_{red}^2	Cov	D.O.F
$[Mn/Fe] = -0.030(40)[Ba/Fe] - 0.220(50)$	2.616	-0.001820	33
$[Cu/Fe] = 0.045(50)[Ba/Fe] - 0.200(60)$	1.072	-0.003206	33
$[Zn/Fe] = 0.160(60)[Ba/Fe] - 0.195(70)$	1.748	-0.004097	33
$[Mn/Fe] = 0.060(40)[Y/Fe] - 0.310(40)$	2.564	-0.001784	33
$[Cu/Fe] = 0.120(60)[Y/Fe] - 0.260(60)$	0.955	-0.003019	33
$[Zn/Fe] = 0.250(70)[Y/Fe] - 0.240(60)$	1.513	-0.004019	33
Least-squares fits for Fig. 4			
	χ_{red}^2	Cov	D.O.F
$[Mn/Fe] = -0.052(30)[Nd/Fe] - 0.210(20)$	2.512	-0.000589	33
$[Cu/Fe] = 0.010(40)[Nd/Fe] - 0.150(30)$	1.095	-0.001122	33
$[Zn/Fe] = 0.185(40)[Nd/Fe] - 0.160(40)$	1.371	-0.001469	33
$[Mn/Fe] = -0.090(60)[Eu/Fe] - 0.220(20)$	2.185	-0.001024	38
$[Cu/Fe] = 0.040(60)[Eu/Fe] - 0.170(20)$	1.893	-0.001006	38
$[Zn/Fe] = 0.370(90)[Eu/Fe] - 0.140(30)$	1.605	-0.002642	38
Least-squares fits for Fig. 5			
	χ_{red}^2	Cov	D.O.F
$[Mn/Fe] = -0.000(40)[Gd/Fe] - 0.250(20)$	2.286	-0.000596	37
$[Cu/Fe] = 0.055(50)[Gd/Fe] - 0.180(30)$	1.008	-0.001135	37
$[Zn/Fe] = 0.290(70)[Gd/Fe] - 0.140(40)$	1.047	-0.001965	37
$[Mn/Fe] = -0.050(30)[Dy/Fe] - 0.230(20)$	2.230	-0.000323	36
$[Cu/Fe] = 0.025(40)[Dy/Fe] - 0.160(20)$	1.070	-0.000630	36
$[Zn/Fe] = 0.180(50)[Dy/Fe] - 0.090(25)$	1.721	-0.000877	36
Least-squares fits for Fig. 8			
	χ_{red}^2	Cov	D.O.F
$[Mn/Fe] = 0.050(40)[Sr/Fe] - 0.300(40)$	2.548	-0.001253	32
$[Cu/Fe] = 0.050(50)[Sr/Fe] - 0.190(40)$	1.017	-0.002009	32
$[Zn/Fe] = 140(60)[Sr/Fe] - 0.130(50)$	1.728	-0.002768	32
$\log \epsilon(Mn) = 1.030(80)\log \epsilon_w(Sr) + 3.020(140)$	0.952	-0.010765	37
$\log \epsilon(Cu) = 0.990(90)\log \epsilon_w(Sr) + 1.990(160)$	0.690	-0.014851	37
$\log \epsilon(Zn) = 0.620(70)\log \epsilon_w(Sr) + 3.180(10)$	1.867	-0.008325	37
$\log \epsilon(Mn) = -0.020(60)\log \epsilon_m(Ba) + 4.840(170)$	6.992	-0.010044	32
$\log \epsilon(Cu) = 0.100(70)\log \epsilon_m(Ba) + 3.410(210)$	4.615	-0.014135	32
$\log \epsilon(Zn) = 0.010(50)\log \epsilon_m(Ba) + 4.200(150)$	4.908	-0.007749	32

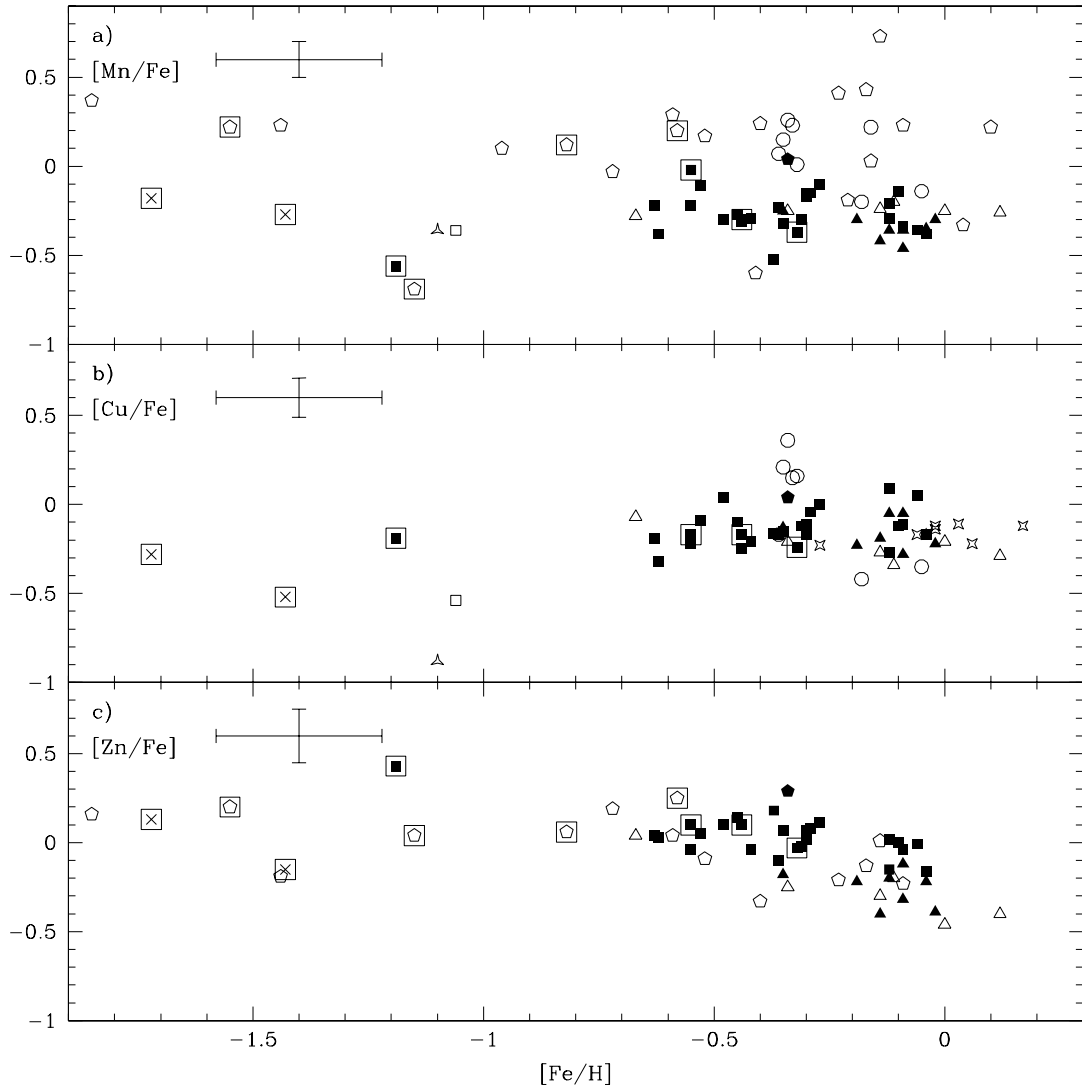


Fig. 1. $[\text{Mn}/\text{Fe}]$, $[\text{Cu}/\text{Fe}]$ and $[\text{Zn}/\text{Fe}]$ vs. $[\text{Fe}/\text{H}]$. Error bars represent the highest values for the uncertainties for each axis. Symbols: triangles are results from this work, where filled triangles are barium stars and open triangles, those stars considered to be normal by Smiljanic et al. (2007); filled squares are data taken from Allen & Barbuy (2006a); filled pentagon: Pereira & Junqueira (2003); crosses: Junqueira & Pereira (2001); open square: BD-21° 3873, a halo symbiotic star of Pereira & Porto de Mello (1997); starred triangle: HE2-467, a halo yellow symbiotic star of Pereira et al. (1998); starred squares: Castro et al. (1999); open pentagons: Luck & Bond (1991); open circles: Smith et al. (1993). Big open squares involving some points indicate the halo barium stars, according to Mennessier et al. (1997).

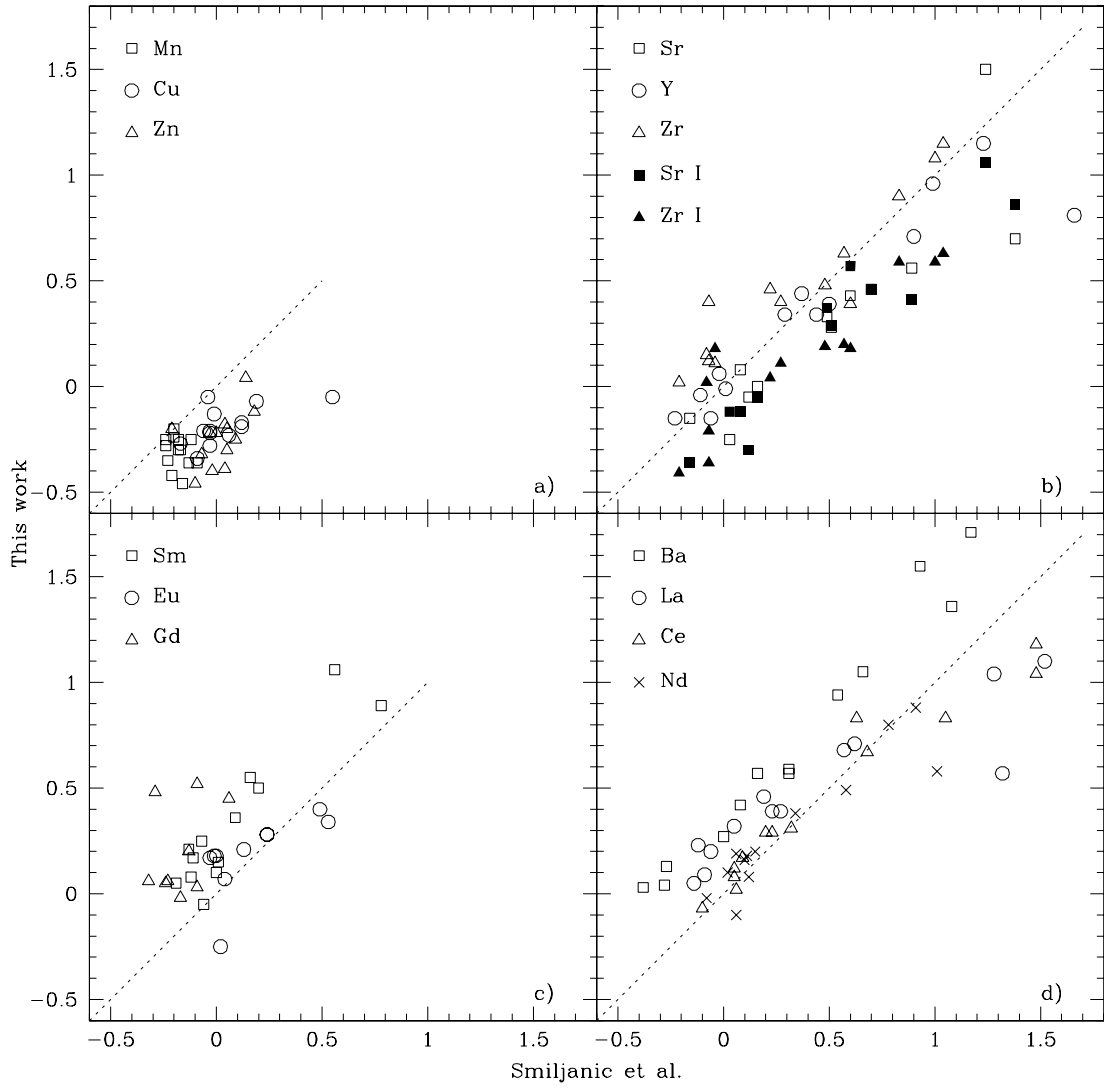


Fig. 2. Comparison between $[X/Fe]$ of Smiljanic et al. (2007) and this work. The dotted lines indicate the same values for both. In panel b) full squares and the full triangles represent the comparison with the average for lines of Sr I and Zr I, respectively, of this work, whereas open squares and triangles represent Sr II and Zr II, respectively.

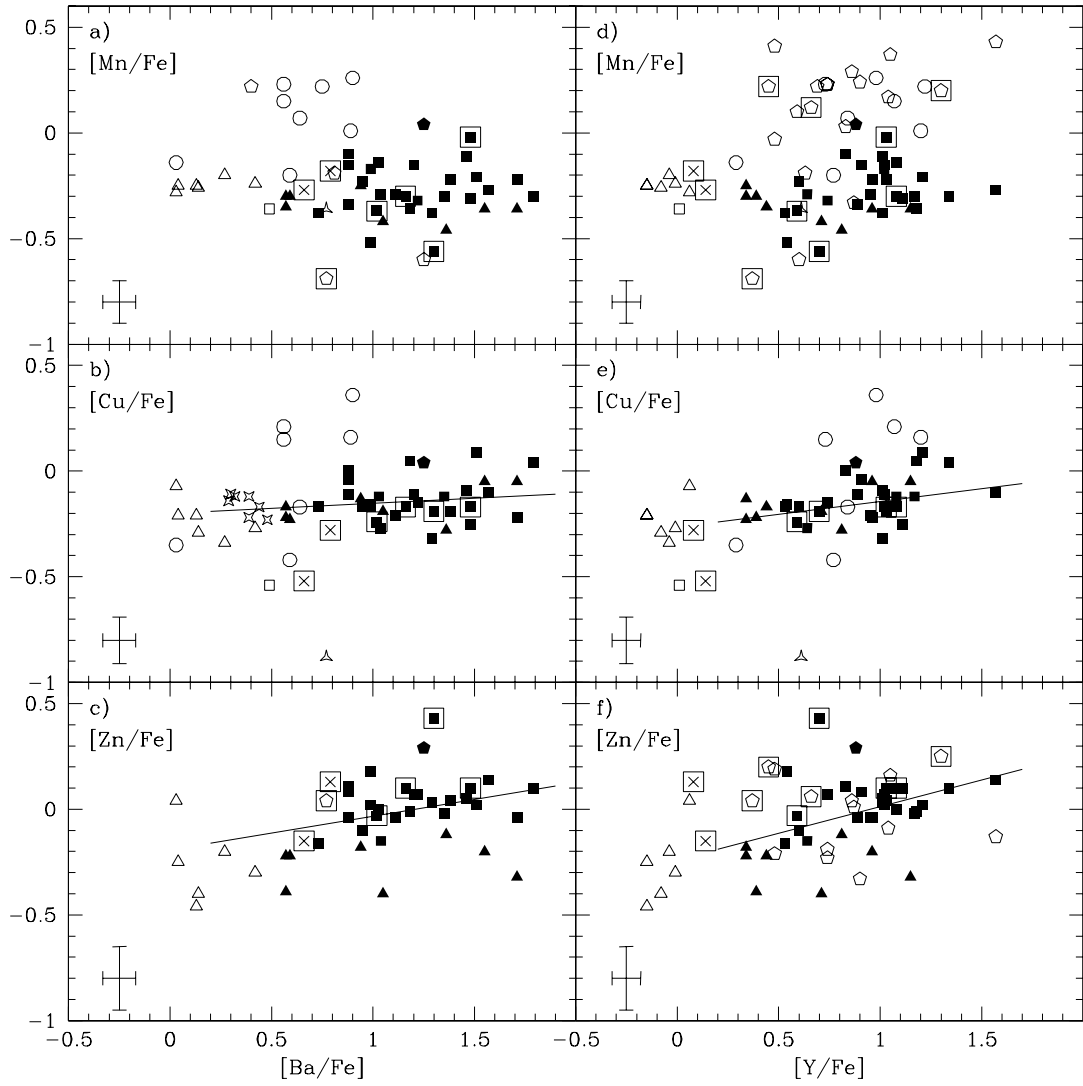


Fig. 3. Abundance ratios involving Mn, Cu, Zn, Ba, Y, and Fe. Error bars are defined as in Fig. 1. Results of the least-squares fits are shown for each panel. Only filled symbols were used in the fits. The straight line is shown only for fits with $\chi_{red}^2 < 2$. Symbols are the same as in Fig. 1. The results for the least-squares fits are given in Table 7.

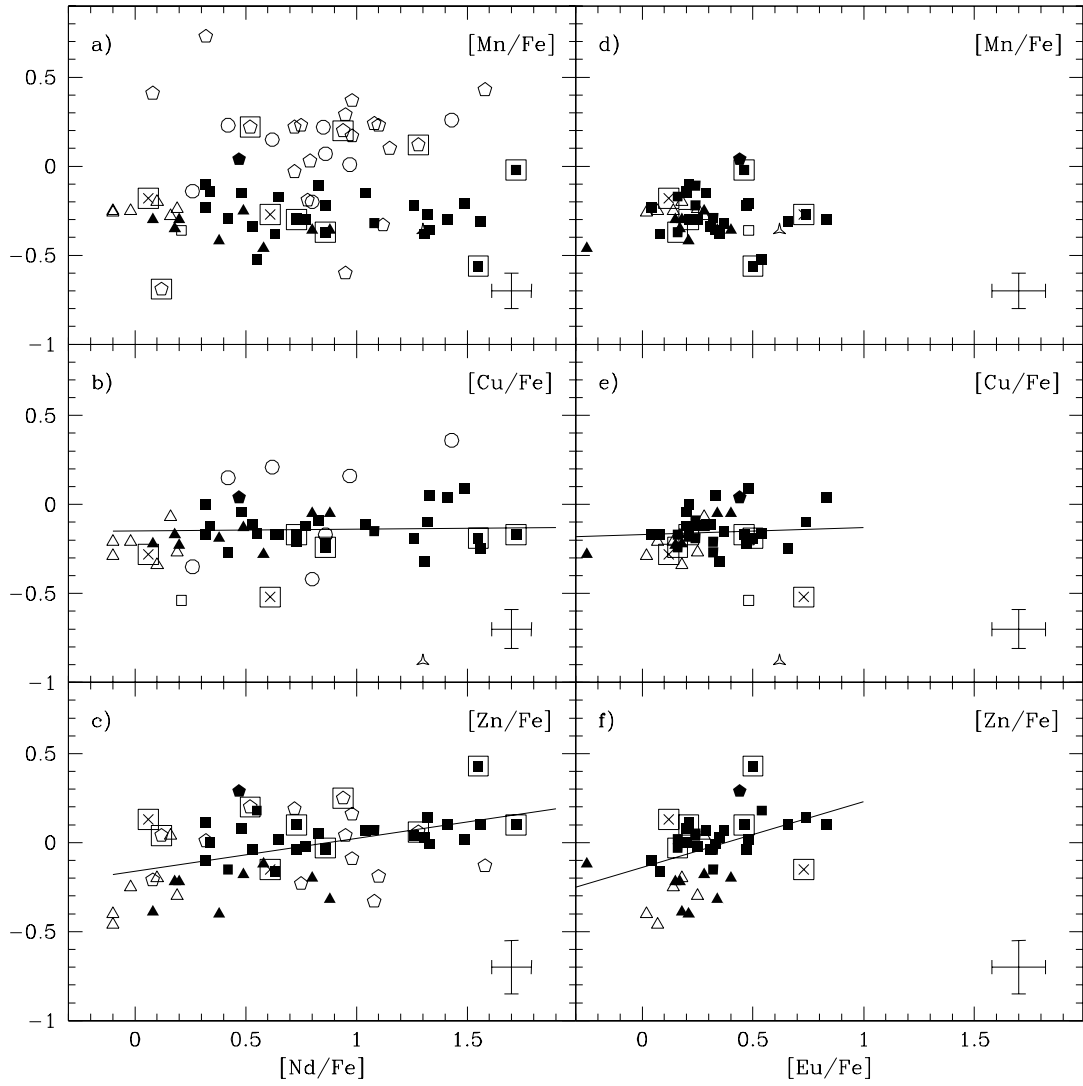


Fig. 4. Abundance ratios involving Mn, Cu, Zn, Nd, Eu, and Fe. Error bars are defined as in Fig. 1. Results of the least-squares fits are shown for each panel. For the fits a), b) and c), only filled symbols were used, and for d), e) and f), normal stars (open triangles) were included, except HD 113226. The straight line is shown only for fits with $\chi^2_{red} < 2$. Symbols are the same as in Fig. 1. The results for the least-squares fits are given in Table 7.

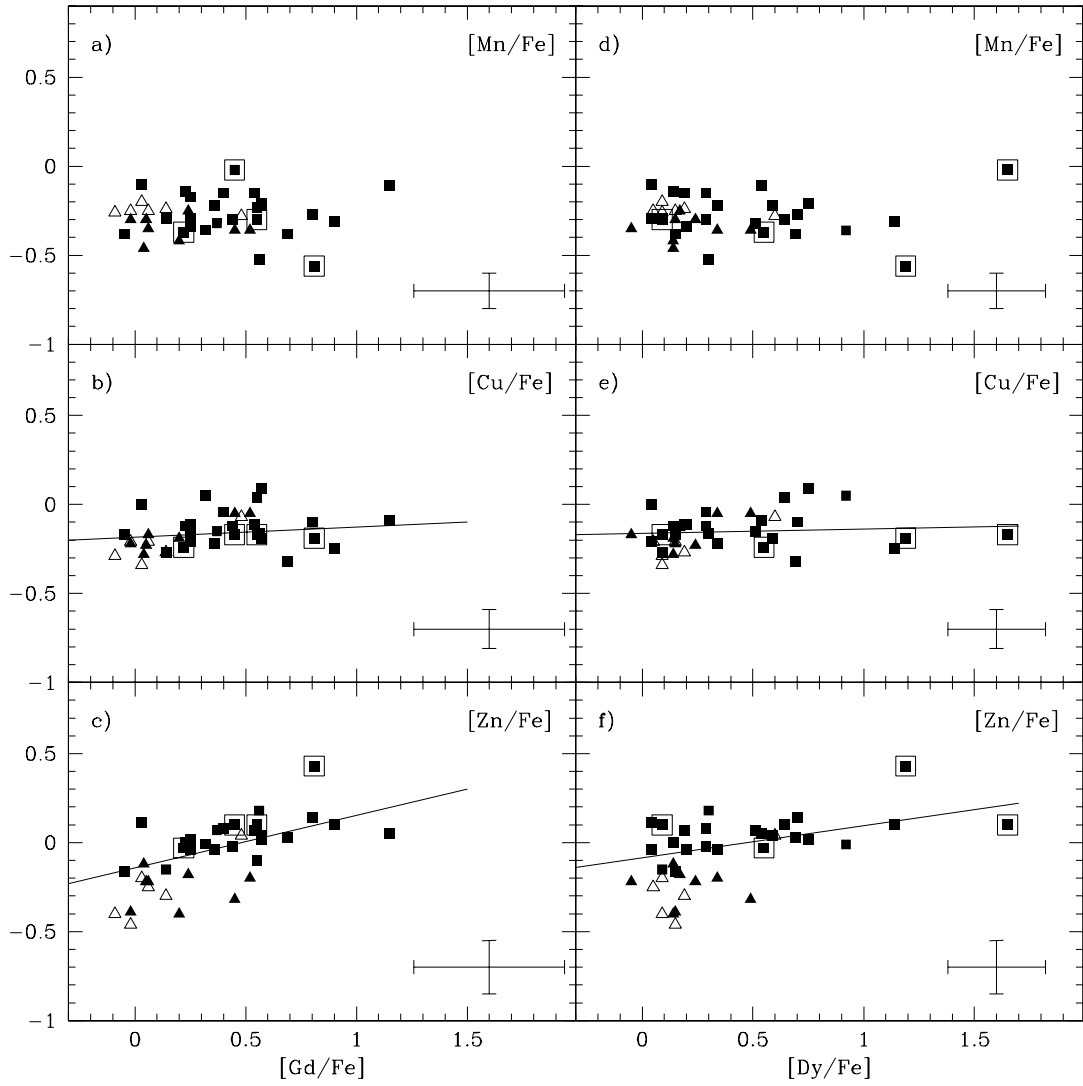


Fig. 5. Abundance ratios involving Mn, Cu, Zn, Gd, Dy, and Fe. Error bars are defined as in Fig. 1. Symbols: triangles are results of this work, where filled are barium stars and open, those stars considered to be normal instead of barium stars by Smiljanic et al. (2007); Filled squares: Allen & Barbuy (2006a). Results of the least-squares fits are shown for each panel. Only filled symbols were used in the fits. The straight line is shown only for fits with $\chi_{red}^2 < 2$. The results for the least-squares fits are given in Table 7.

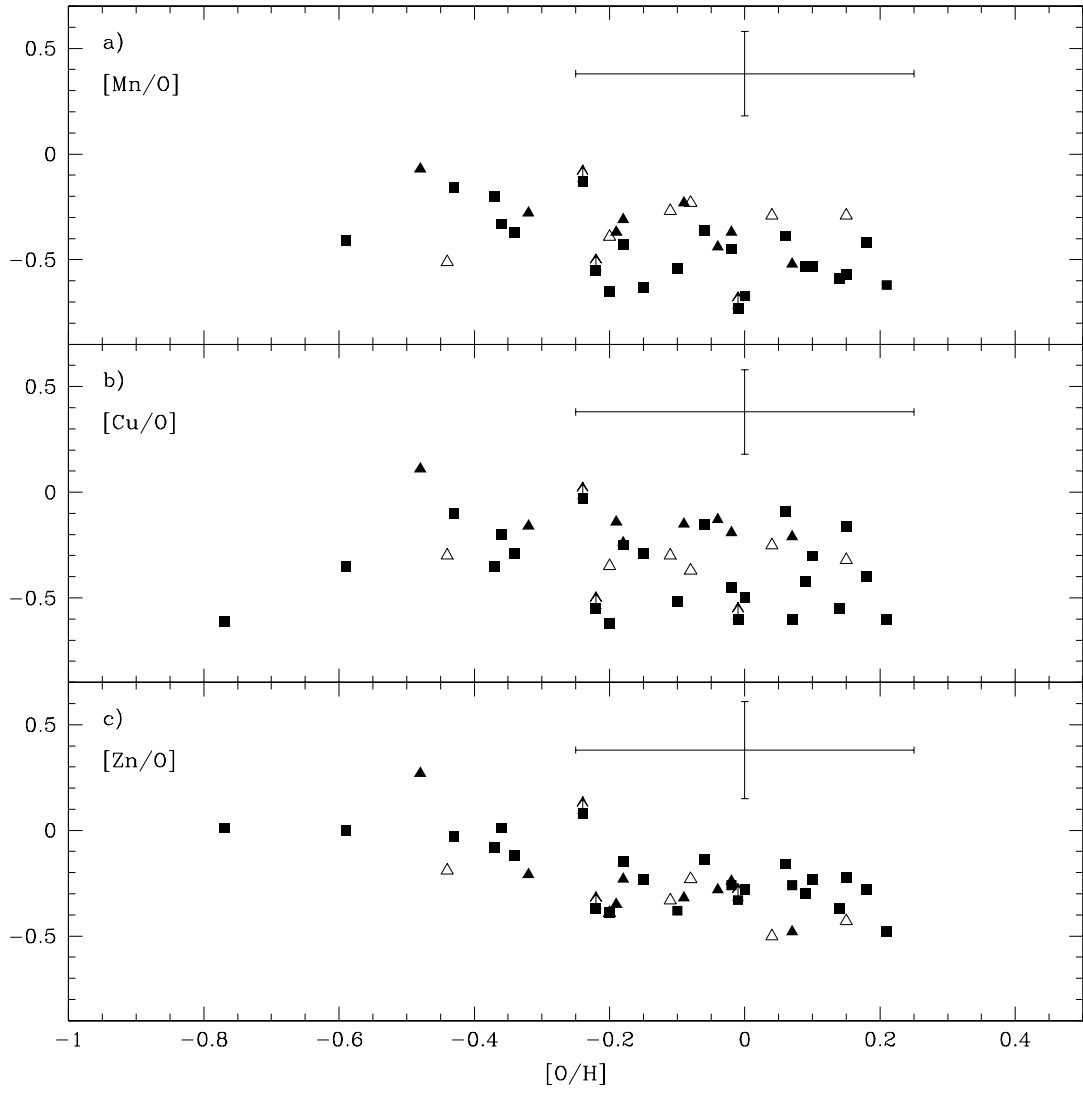


Fig. 7. $[Mn/O]$, $[Cu/O]$ and $[Zn/O]$ vs. $[O/H]$. Error bars are defined as in Fig. 1. Arrows up indicate lower limits for the ratios. Symbols: triangles are results of this work, where filled are barium stars and open, those stars considered to be normal instead of barium stars by Smiljanic et al. (2007); filled squares are data taken from Allen & Barbuy (2006a).

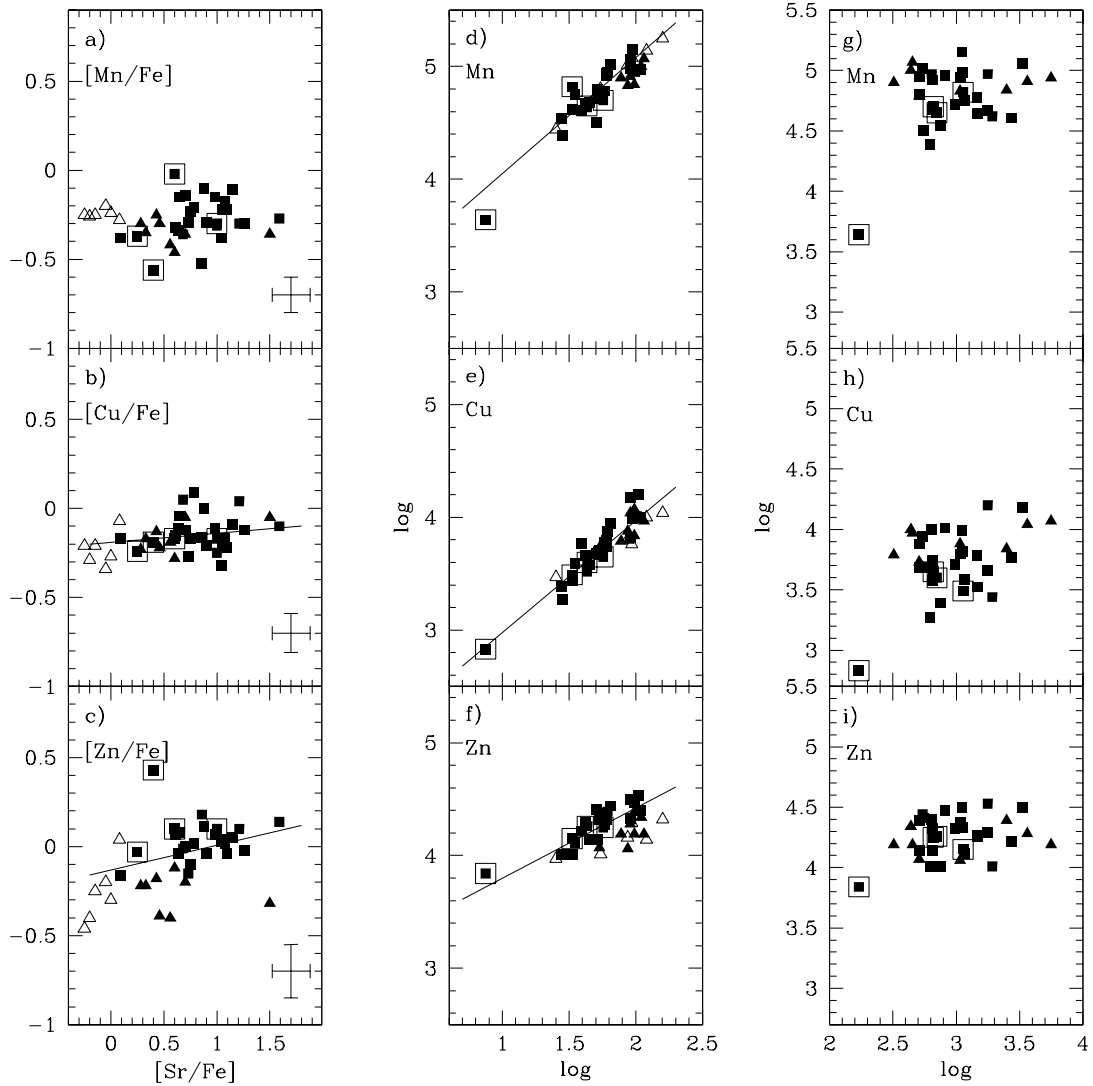


Fig. 8. Symbols are the same as in Fig. 7. Panels a), b) and c) show $[Mn, Cu, Zn/Fe]$ vs. $[Sr/Fe]$. The least-squares fits used only filled symbols. Panels d), e) and f) show $\log \epsilon(X)$, where X is Mn, Cu, or Zn as a function of the logarithmic part of the fraction of Sr abundance with regard to the weak component of the s -process. The least-squares fits used all symbols. Panels g), h) and i) show $\log \epsilon(X)$, where X is Mn, Cu, or Zn as a function of the logarithmic part of the fraction of Ba abundance relative to the main component of the s -process. The least-squares fits used only filled symbols. The results for the least-squares fits are given in Table 7.